JOURNAL OF COMPUTATIONAL PHYSICS 27, 103–122 (1978)

A Locally Two-Dimensional Numerical Method for Calculating Three-Dimensional Supersonic Flows

F. WALKDEN, P. CAINE, AND G. T. LAWS

Department of Mathematics, University of Salford, England

Received January 11, 1977; revised May 25, 1977

A finite difference method of calculating steady supersonic flow of an inviscid ideal gas is described for the case in which a boundary condition has to be satisfied at the surface of any given complicated body shape. The supersonic flow equations are formulated in an arbitrary non-orthogonal co-ordinate system and an operator splitting method is used to construct discrete representations of the equations of motion. Results are presented to demonstrate that the method is capable of capturing shock waves satisfactorily and that it produces results in agreement with other theoretical results. Comparisons between numerical and experimental results for an intake cowl shape, which has a sharp corner and which is representative of a class of complicated body shapes of practical interest, indicates that the method can be relied upon to produce accurate results for complicated body shapes.

1. INTRODUCTION

A comprehensive list of existing methods of calculating steady inviscid supersonic supersonic flow fields is provided in a recent review paper by Taylor [1]. Although the number of existing methods is very large, new methods that are more efficient, more robust and more flexible in operation than existing methods are being sought at present.

The finite difference method described here is a contribution to current research aimed at the production of satisfactory new flow calculation methods for different types of body shapes associated with aircraft configurations. Although efficiency, robustness and flexibility requirements conflict one with another, none is ignored in the method described here.

For the present discussion, it is useful to distinguish two lines of development of supersonic flow calculation methods. One consists of methods based on the theory of characteristics, for example those described by Chu [2] and Butler [3], in which shock waves are fitted as discontinuities. The other consists of methods, stemming from Lax's method [4], based on equations of motion consisting of conservation laws formulated as divergence expressions, for example the method described by Kutler and Lomax [5]. Other methods relevant in the discussion here are ones which may be regarded as hybrids of the two lines described above. The method used by Marconi and Salas [6], a method derived from earlier work by Moretti *et al.* [7], is one such method in which all shock waves are fitted as discontinuities but the flow between shock waves and

0021-9991/78/0271-0103$02.00/0

boundaries of the flow-field is calculated using the MacCormack [8] method based on divergence expressions of conservation laws. The method described in this paper is also hybrid in the sense in which the term is used here. Although certain shock waves, e.g. bow shock waves, may be treated as discontinuities, the method presented is essentially a shock capturing finite difference method, but the finite difference equations are derived by using the theory of characteristics rather than by using equations of motion formulated as divergence expressions.

Marconi and Salas calculated steady supersonic flows associated with certain typical aircraft configurations. They used the second order finite difference method of MacCormack [8] and employed a numerical conformal transformation technique to construct suitable co-ordinate systems. A characteristics-type procedure was employed to calculate the flow at points on boundary surfaces, and shock waves were treated as discontinuities.

In contrast to the other numerical methods, that described in this paper is based on a formulation of the equations of motion which allows the use of arbitrary non-orthogonal co-ordinate systems but does not contain any derivatives of elements of the metric tensor. One result of this choice of formulation is that the equations of motion are not divergence expressions. Therefore, it is not possible to apply methods such as the well known MacCormack method for computing second order finite difference solutions. Instead, a first order method [9], based on approximations to characteristic relations for a pair of two-dimensional systems of equations, is used. These two-dimensional systems are derived from the full equations by an operator splitting method—see Section 3. Apart from its practical value, the operator splitting method is of academic interest. It is different from those described in the definitive monograph by Yanenko [10].

The equations of motion are formulated in terms of an arbitrary non-orthogonal co-ordinate system in order to achieve flexibility. This formulation allows the relatively straight-forward treatment of many different classes of body shapes without a need for extensive re-writing of the part of the computer program concerned with the computational algorithm. The user of the program has to specify only three functions to describe a body-orientated co-ordinate system in space. This co-ordinate system may be formed by combining several sub-systems associated with different parts of a body surface, and the simplest imaginable sub-systems appear to work satisfactorily in practice.

The formulation of equations of motion which do not contain derivatives of elements of the metric tensor is used in order to achieve good overall computational efficiency. Divergence forms of the equations of motion in general co-ordinate systems do contain derivatives of elements of the metric tensor. Systems of this type were investigated before the present formulation was derived, and it was found that large amounts of time had to be spent computing elements of the metric tensor and their derivatives. The general procedure of the present method, in which a body-orientated co-ordinate system is obtained by simple algebraic operations, is more economical than the conformal transformation procedure described by Marconi and Salas [6]. Although the gains are counter-balanced to some extent by our use of

a first order finite difference scheme, the overall efficiency of the method is acceptable.

A finite difference method derived from the theory of characteristics was chosen in order to achieve uniformity in the calculation of the flow at interior mesh points and at finite difference mesh points on boundary surfaces. We believe that this uniformity contributes to the robustness of numerical methods. When divergence law formulations of the equations of motion are used, the application of boundary conditions generally leads to non-uniformity in the treatment of interior and boundary points.

The first order finite difference method was used because previous work suggested that this particular technique would lead to a method that would capture shock waves satisfactorily. In spite of widely held views to the contrary, there are some numerical methods based on equations of motion that are not formulated as divergence expressions which can capture shock waves automatically by smoothing discontinuities before they are fully developed. Methods, similar to the present one, derived using characteristics belong to this class. Some numerical evidence showing that the method of this paper can capture shock waves is given in Section 7. Additional evidence is available in two papers by Walkden and Caine [9, 11], in a paper by Walkden *et al.* [12], and in a paper by Garabedian and Korn [13].

The numerical methods of the present paper were specially devised to treat the intake cowl problem described in Section 6. In this problem the body shape cannot be mapped simply onto a single co-ordinate surface in some computational working space. The locally two-dimensional method was first used in January 1974 to consider the intake cowl problem described in this paper. Since that date the method has been used to calculate steady supersonic flow fields for bodies from a number of other classes: aircraft fuselages, fuselage and cockpit-canopy combinations, wings, turbomachinery blade rows, the tips of rotating and translating helicopter blades. For some of these problems, bow shock waves have been fitted as discontinuities. In others, however, all the shock waves have been captured. In the latter case, the shock discontinuities have been smoothed.

2. Equations of Motion

The formulation of the equations of motion given here in Eqs. (1) is for a general system of orthogonal co-ordinates.

Momentum:

$$\begin{aligned}
&\frac{u_1}{h_1}\frac{\partial u_1}{\partial x^1}+\frac{u_2}{h_2}\frac{\partial u_1}{\partial x^2}+\frac{u_3}{h_3}\frac{\partial u_1}{\partial x^3}+\frac{1}{\rho}\frac{\partial p}{\partial x^1}=r_1\,,\\
&\frac{u_1}{h_1}\frac{\partial u_2}{\partial x^1}+\frac{u_2}{h_2}\frac{\partial u_2}{\partial x^2}+\frac{u_3}{h_3}\frac{\partial u_2}{\partial x^3}+\frac{1}{\rho}\frac{\partial p}{\partial x^2}=r_2\,,\\
&\frac{u_1}{h_1}\frac{\partial u_3}{\partial x^1}+\frac{u_2}{h_2}\frac{\partial u_3}{\partial x^2}+\frac{u_3}{h_3}\frac{\partial u_3}{\partial x^3}+\frac{1}{\rho}\frac{\partial p}{\partial x^3}=r_3\,.
\end{aligned}\tag{1}$$

The dependent variables u_1, u_2, u_3 are velocity components in x^1, x^2, x^3 space. Expressions for h_i and r_i, $i = 1, 2, 3$, in different co-ordinate systems, are given in Appendix 1.

We define

$$\tau_j^{\ i} = h_i \frac{\partial x^i}{\partial \eta^j}, \qquad \tau_j^{*i} = \frac{1}{h_j} \frac{\partial \eta^i}{\partial x^j},$$

$$v_i = \sum_j u_j \tau_i^{\ j}, \tag{2}$$

$$v^i = \sum_j u_j \tau_j^{*i}.$$

Then

$$\sum v_i \tau_k^{*i} = u_k \qquad \text{and} \qquad \sum_i v^i \tau_i^{\ k} = u_k,$$

$$v_i = \sum_j g_{ij} v^j, \tag{3}$$

$$v^i = \sum_j g^{ij} v_j.$$

Stratton [14] provides derivations of Eqs. (3) and other useful equations associated with non-orthogonal co-ordinate systems.

Equations (1) may be re-written in a modified form with η^1, η^2, η^3 as independent variables in place of x^1, x^2 and x^3:

$$\begin{aligned} v^1 \frac{\partial u_1}{\partial \eta^1} + v^2 \frac{\partial u_1}{\partial \eta^2} + v^3 \frac{\partial u_1}{\partial \eta^3} + \frac{1}{\rho} \frac{\partial p}{\partial \eta^\alpha} \frac{\partial \eta^\alpha}{\partial x^1} &= r_1, \\ v^1 \frac{\partial u_2}{\partial \eta^1} + v^2 \frac{\partial u_2}{\partial \eta^2} + v^3 \frac{\partial u_2}{\partial \eta^3} + \frac{1}{\rho} \frac{\partial p}{\partial \eta^\alpha} \frac{\partial \eta^\alpha}{\partial x^2} &= r_2, \\ v^1 \frac{\partial u_3}{\partial \eta^1} + v^2 \frac{\partial u_3}{\partial \eta^2} + v^3 \frac{\partial u_3}{\partial \eta^3} + \frac{1}{\rho} \frac{\partial p}{\partial \eta^\alpha} \frac{\partial \eta^\alpha}{\partial x^3} &= r_3. \end{aligned} \tag{4}$$

We may write $u_k = \sum_{i=1}^{3} \bar{v}_i \bar{\tau}_k^{*i}$ where $\bar{\tau}_k^{*i}$ denotes the constant values of τ_k^{*i} at any fixed point P in space. Thus, for any given flow field, since the velocity components, u_k, $k = 1, 2, 3$, vary with position in space it follows that the co-variant velocity components $\bar{v}_i$ will vary with position in space and with the position of the point P. Thus it follows that Eqs. (4) are equivalent to

$$\sum_\beta v^\beta \frac{\partial \bar{v}_\delta}{\partial \eta^\beta} + \frac{1}{\rho} \sum_\epsilon \sum_\alpha \frac{\partial p}{\partial \eta^\alpha} \bar{\tau}_\epsilon^{*\alpha} \bar{\tau}_\delta^{\ \epsilon} = k_\delta, \qquad \delta = 1, 2, 3, \tag{5}$$

where

$$k_\delta = \sum_\epsilon \bar{\tau}_\delta^{\ \epsilon} r_\epsilon. \tag{6}$$

Conservation of Mass and Entropy

In terms of the independent variables η^1, η^2 and η^3, the equations of conservation of mass and entropy respectively may be expressed in the following form:

$$\sum_{\epsilon}\sum_{\beta}\sum_{\alpha}\tau_{\beta}^{*\alpha}\tau_{\beta}^{\epsilon}\frac{\partial}{\partial\eta^{\alpha}}(\rho\bar{v}_{\epsilon}) = \rho k_4\,, \tag{7}$$

$$\sum_{\alpha} v^{\alpha}\frac{\partial}{\partial\eta^{\alpha}}\left(\frac{p}{\rho^{\nu}}\right) = 0. \tag{8}$$

3. Further Analysis of the Equations of Motion

Here we describe an analysis of Eqs. 2(5), 2(7) and 2(8) for the case of supersonic flow when the equations form a hyperbolic system. The analysis leads to expressions for η^1-derivatives in terms of η^2 and η^3-derivatives of the dependent variables p, ρ, $\bar{v}_{\epsilon}$, $\epsilon = 1, 2, 3$. These expressions form the basis of the numerical method investigated in this paper.

A first-order finite difference technique will be used and to this order of accuracy, in the neighborhood of a point P, equations 2(5), 2(7) and 2(8) can be approximated by simpler equations:

$$\sum_{\beta}\left\{\bar{v}^{\beta}\frac{\partial\bar{v}_{\delta}}{\partial\eta^{\beta}} + \frac{1}{\rho}\frac{\partial p}{\partial\eta^{\delta}}\right\} = k_{\delta}\,, \qquad \delta = 1, 2, 3, \tag{1}$$

$$\sum_{\epsilon}\sum_{\alpha}\bar{g}^{\alpha\epsilon}\frac{\partial}{\partial\eta^{\alpha}}(\rho\bar{v}_{\epsilon}) = \rho k_4\,, \tag{2}$$

$$\sum_{\alpha}\bar{v}^{\alpha}\frac{\partial}{\partial\eta^{\alpha}}(p/\rho^{\nu}) = 0. \tag{3}$$

Elimination of density derivatives between Eqs. (2) and (3) leads to equations which can be combined into a single matrix equation:

$$A\frac{\partial u}{\partial\eta^1} + B\frac{\partial u}{\partial\eta^2} + C\frac{\partial u}{\partial\eta^3} = k, \tag{4}$$

where A, B, and C are 4×4 matrices, and u and k are vectors:

$$u = (\bar{v}_1\,, \bar{v}_2\,, \bar{v}_3\,, p).$$

The matrices A, B and C are given in Appendix 2.

Equation (4) splits into two parts:

$$\frac{1}{2}A\frac{\partial u}{\partial \eta^1} + B\frac{\partial u}{\partial \eta^2} = \frac{1}{2}k, \tag{5a}$$

$$\frac{1}{2}A\frac{\partial u}{\partial \eta^1} + C\frac{\partial u}{\partial \eta^3} = \frac{1}{2}k, \tag{5b}$$

One part contains no η^3-derivatives, and the other part contains no η^2-derivatives.

Now, provided the components of velocity in the $(\eta^1 - \eta^2)$ and $(\eta^1 - \eta^3)$ planes at P are supersonic, Eqs. (5a) and (5b) are hyperbolic. Then these can be represented in characteristic form:

$$\frac{\partial}{\partial \zeta^1}\left(\frac{\bar{v}_1}{2}\right) + \frac{\bar{v}^j}{\bar{v}^1}\frac{\partial}{\partial \zeta^1}\left(\frac{\bar{v}_j}{2}\right) + \frac{1}{\rho \bar{v}^1}\frac{\partial}{\partial \zeta^1}\left(\frac{p}{2}\right) = \frac{0.5}{\bar{v}^1}\left\{k_1 + \frac{\bar{v}^j}{\bar{v}^1}k_j\right\}, \tag{6}$$

$$\frac{\partial}{\partial \zeta^1}\left(\frac{\bar{v}_m}{2}\right) = \frac{0.5}{\bar{v}^1}k_m, \tag{7}$$

$$\left(\sum_i d_i{}^j a_{i1}\right)\frac{\partial}{\partial \zeta^1}\left(\frac{\bar{v}_1}{2}\right) + \left(\sum_i d_i{}^j a_{i2}\right)\frac{\partial}{\partial \zeta^1}\left(\frac{\bar{v}_2}{2}\right) + \left(\sum_i d_i{}^j a_{i3}\right)\frac{\partial}{\partial \zeta^1}\left(\frac{\bar{v}_3}{2}\right) + \left(\sum_i d_i{}^j a_{i4}\right)\frac{\partial}{\partial \zeta^1}\left(\frac{p}{2}\right) = \frac{1}{2}\left(\sum_i d_i{}^j k_i\right). \tag{8}$$

In Eqs. (6) and (7),

$$\frac{\partial}{\partial \zeta^1} = \frac{\partial}{\partial \eta^1} + \frac{2\bar{v}^j}{\bar{v}^1}\frac{\partial}{\partial \eta^j}. \tag{9}$$

Equation (8) represents two characteristic relations in which

$$\frac{\partial}{\partial \zeta^1} = \frac{\partial}{\partial \eta^1} + 2\mu\frac{\partial}{\partial \eta^j} \tag{10}$$

$$d_i{}^j = \mu \bar{g}^{i1} - \bar{g}^{ij}, \qquad i = 1, 2, 3, \tag{11}$$

$$d_4{}^j = \bar{v}^j - \mu \bar{v}^1, \tag{12}$$

for $\mu = \mu_+{}^j$ and $\mu = \mu_-{}^j$ respectively, where

$$\mu_\pm{}^j = \frac{\left(g^{1j} - \dfrac{\bar{v}^1\bar{v}^j}{(a)^2}\right) \pm \left\{(\bar{g}^{1j})^2 - \dfrac{2\bar{g}^{1j}\bar{v}^1\bar{v}^j}{(a)^2} - \bar{g}^{11}\bar{g}^{jj} + g^{jj}\dfrac{(\bar{v}^1)^2}{(a)^2} + \bar{g}^{11}(\bar{v}^j)^2/(a)^2\right\}^{1/2}}{(\bar{g}^{11} - (\bar{v}^1)^2/(a)^2)} \tag{13}$$

The characteristic equations equivalent to (5a) are obtained by putting $j = 2$ and $m = 3$ in Eqs. (6)–(13). Those equivalent to (5b) are obtaining by putting $j = 3$ and $m = 2$. The analysis leading to Eqs. (6)–(13) is straightforward in principle and so it has been omitted.

Now the four equations (6)–(8) may be written in the form

$$A_j \frac{\partial}{\partial \eta^1}\left(\frac{u}{2}\right) = B_j \frac{\partial u}{\partial \eta^j} + R_j \tag{14}$$

provided a suitable choice of elements for the 4-vector R_j and for the 4×4 matrices A_j and B_j is made.

Then, formally, each of the two sets of systems of equations (14), for which $j = 2$ and $j = 3$ respectively, can be solved for $(\partial/\partial\eta^1)(u/2)$ and the results combined to obtain

$$\frac{\partial u}{\partial \eta^1} = B_4 \frac{\partial u}{\partial \eta^2} + C_4 \frac{\partial u}{\partial \eta^3} + R_4 \tag{15}$$

where

$$\begin{aligned} B_4 &= A_2^{-1} B_2 , \\ C_4 &= A_3^{-1} C_3 , \\ R_4 &= A_2^{-1} R_2 + A_3^{-1} R_3 . \end{aligned} \tag{16}$$

4. Finite Difference Equations

This section contains a brief account of basic ideas used in constructing finite difference approximations to the characteristic equations described in Section 3.

The coefficients of $\partial u/\partial\eta^1$, $\partial u/\partial\eta^2$, $\partial u/\partial\eta^3$ and the elements of the vectors R_2 and R_3 in equations 3(14) for $j = 2, 3$ are all functions of p, ρ, u_1, u_2, u_3, $\bar{\tau}_j^{\,i}$ and $\bar{\tau}_j^{*i}$ $(i, j = 1, 2, 3)$. In flows where shock waves occur, these functions are evaluated using average values of p, ρ, u_1, u_2, and u_3.

Prior to solving Eqs. 3(14) to obtain numerical estimates for $\partial u/\partial\eta^1$ at a point (i, j, k) in space, the partial derivatives $\partial u/\partial\eta^j$, for $j = 2$ and 3, have to be replaced by appropriate finite difference approximations. This is generally done by a first-order forward difference approximation if the coefficient of the derivative is negative or zero, and by a first-order backward difference approximation if the coefficient is positive. A justification of this procedure for constructing finite difference approximations to characteristic relations has been given by Courant *et al.* [15]. Average values of p, or u_m for $m = 1, 2, 3$, at the point (i, j, k), say, are used in finite difference approximations to derivatives in the equations of motion at (i, j, k). For example, $(\partial p/\partial\eta^2)_{i,j,k}$ may be approximated by

$$(p_{i,j+1,k} - \bar{p}_{i,j,k})/\Delta\eta^2 \qquad \text{or by} \qquad (\bar{p}_{i,j,k} - p_{i,j-1,k})/\Delta\eta^2.$$

5. Calculation Procedures

5.1. *Field Points*

The values of the dependent variables p, ρ, u^1, u^2 u^3 can be predicted at the point $(i+1\ j, k)$ provided they are known at the five points (i, j, k), $(i, j \pm 1, k)$, $(i, j, k \pm 1)$. $\{(\partial/\partial\eta^1)(u/2)\}^{(s)}_{i,j,k}$ is evaluated from Eq. 3(14) for $s = 2, 3$, and then

$$u_{i+1,j,k} = \bar{u}_{i,j,k} + \left[\left\{\frac{\partial}{\partial\eta^1}\left(\frac{u}{2}\right)\right\}^{(2)}_{i,j,k} + \left\{\frac{\partial}{\partial\eta^1}\left(\frac{u}{2}\right)\right\}^{(3)}_{i,j,k}\right] \Delta\eta^1. \tag{1}$$

Once $p_{i+1,j,k}$ and $(v_m)_{i+1,j,k}$, $m = 1, 2, 3$, i.e., the elements of $u_{i+1,j,k}$, have been calculated, the values of $(u_m)_{i+1,j,k}$, $m = 1, 2, 3$, can be obtained simply by repeated application of the first of Eqs. 2(3).

The value of $\rho_{i+1,j,k}$ may be obtained in a number of ways of which two are given here. Employing the energy equation yields

$$\rho_{i+1,j,k} = \left\{\frac{\gamma p}{(\gamma-1)[H - \frac{1}{2}((u_1)^2 + (u_2)^2 + (u_3)^2)]}\right\}_{i+1,j,k} \tag{2}$$

when H is a known universal constant for the flow.

Alternatively,

$$\rho_{i+1,j,k} = \left\{p_{i+1,j,k}\Big/\left(\frac{p}{\rho^\gamma}\right)_{i+1,j,k}\right\}^{1/\gamma} \tag{3}$$

where $(p/\rho^\gamma)_{i+1,j,k}$ may be obtained, for example, from Eq. 2(8) by numerical integration.

5.2. *Boundary Points*

By making suitable choices of transformation functions $x^i = x^i(\eta^1, \eta^2, \eta^3)$, it can be ensured that boundary conditions have to be applied only on surfaces represented by planes in the working space (η^1, η^2, η^3). Several types of boundary conditions may be distinguished. For example, there are some boundaries at which the flow is known, there are some at which a symmetry condition has to be applied, there are some at which shock relations have to be satisfied and there are others at which a condition of zero flow through a solid surface has to be applied. The treatment of uniform flow and symmetry boundaries is straightforward.

At a shock or solid surface boundary, certain characteristic relations are replaced by boundary conditions. Here to fix ideas, a description is given of the procedure followed when a solid surface boundary condition is applied at $\eta^2 = 0$.

If $\mathbf{N}$ is a vector normal to the solid surface at $(i+1, 0, k)$ then

$$[(\bar{v}_1\mathbf{a}^1 + \bar{v}_2\mathbf{a}^2 + \bar{v}_3\mathbf{a}^3)_{i+1,j,k}] \cdot \mathbf{N} = 0 \tag{4}$$

where the vectors $\mathbf{a}^1$, $\mathbf{a}^2$ and $\mathbf{a}^3$ are normals to the co-ordinate surfaces $\eta^1 =$ constant, $\eta^2 = 0$ and $\eta^3 =$ constant at the point $(i + 1, 0, k)$.

In Eq. (4), $\bar{v}_m$, $m = 1, 2, 3$ is replaced by the expression

$$(\bar{v}_m)_{i,j,k} + \frac{\Delta\eta^1}{2}\left\{\left(\frac{\partial}{\partial\eta^1}(\bar{v}_m)\right)^{(2)}_{i,j,k} + \left(\frac{\partial}{\partial\eta^1}(\bar{v}_m)\right)^{(3)}_{i,j,k}\right\} \tag{5}$$

in which $((\partial/\partial\eta^1)(\bar{v}_m))^{(3)}_{i,j,k}$ is obtained as part of the solution of finite difference representations of Eqs. 3(14) when $j = 3$.

The resulting equation, together with three of the finite difference representations of Eqs. 3(14) with $j = 2$ may then be used to obtain values for the elements of the vector

$$\left\{\frac{\partial}{\partial\eta^1}\left(\frac{u}{2}\right)\right\}^{(2)}_{i,j,k}.$$

The three equations used are those remaining after that corresponding to the left hand characteristic relation (Eq. 3(8) with $j = 2$ and $\mu = \mu_-$) has been omitted in favour of the boundary condition treated according to the procedure outlined here.

Once $\{(\partial/\partial\eta^1)(u/2)\}^{(2)}_{i,0,k}$ and $\{(\partial/\partial\eta^1)(u/2)\}^{(3)}_{i,0,k}$ have been evaluated, values of p, ρ, u_1, u_2, u_3 at $(i + 1, 0, k)$ can be obtained by using the procedure described earlier for field points.

5.3. *Theoretical Justification of the Splitting Method and Analysis of Stability*

Caine [16] has carried out a detailed theoretical study of a numerical procedure based on the following splitting of Eqs. 3(4)

$$\begin{aligned} \alpha_2 A\frac{\partial u}{\partial\eta^1} + B\frac{\partial u}{\partial\eta^2} &= \alpha_2\mathbf{k}, \\ \alpha_3 A\frac{\partial u}{\partial\eta^1} + C\frac{\partial u}{\partial\eta^3} &= \alpha_3\mathbf{k}, \end{aligned} \tag{6}$$

where α_2 and α_3 are positive constants such that $\alpha_2 + \alpha_3 = 1$. He derived equations corresponding to 3(15) and proved that these equations are *identical* to equations 3(4) for $\partial u/\partial\eta^1$ for all α_2 and α_3 such that $\alpha_2 + \alpha_3 = 1$. Now, of course, in the special case of interest here, when $\alpha_2 = \alpha_3 = \frac{1}{2}$, the same result follows. That is, Eq. 3(15) is identical to 3(4).

Caine [16] also carried out a linear stability analysis and showed that a numerical procedure, such as that described here, based on analysis of equations of the form of (6) above, is conditionally stable. The amplification matrix of the three-dimensional numerical procedure is

$$G = \alpha_2 G^{(2)} + \alpha_3 G^{(3)}$$

where $G^{(2)}$ and $G^{(3)}$ are the amplification matrices for numerical procedures based on

the $(\eta^1 - \eta^2)$ and $(\eta^1 - \eta^3)$ split equations. He then used the known stability conditions for the two-dimensional methods to obtain the following sufficient conditions for stability of the three-dimensional procedure:

$$\Delta\eta^1 \leqslant \min\left\{\alpha_2 \frac{\Delta\eta^2}{|w_2|}, \alpha_3 \frac{\Delta\eta^3}{|w_3|}\right\} \tag{7}$$

where $|w_2|$ is the eigenvalue of maximum modulus determined from the equation

$$|B - wA| = 0$$

and $|w_3|$ is the eigenvalue of maximum modulus determined from the equation

$$|C - wA| = 0.$$

6. An Intake Cowl Problem

6.1. *Intake Cowl Geometry*

Shapes belonging to the family of interest here are defined by the parameters b, h_0 and θ_b shown in Fig. 1.

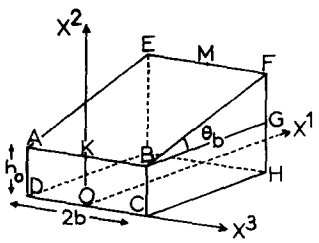

Fig. 1. Schematic diagram of the intake cowl geometry.

6.2. *The Flow Calculation Problem*

Given a uniform supersonic flow at a specified Mach number in the direction of the x^1-axis shown in Fig. 1, the problem is to compute the disturbance produced by the given intake cowl shape. The boundary conditions to be applied are that there is no flow through the boundary surface of the intake and that the flow is symmetrical about the plane $x^2 = 0$ for $x^3 \geqslant b$ and the plane $x^3 = 0$ for $x^2 \geqslant h_0 + x^1 \tan\theta_b$. In addition, of course, the values of the dependent variables p, ρ, u_1, u_2, u_3 are known on the plane $x^1 = 0$.

The flow field produced by the intake cowl has three features worth noting:

(a) The disturbance to the uniform flow propagates outwards away from the cowl

surface with increasing x^1 so, for any given value of $x^1 < L$, the flow will be uniform for large enough values of $(x^2)^2 + (x^3)^2$.

(b) On the upper surface of the intake cowl, starting at its leading edge, a core of two-dimensional flow produced by turning the given uniform flow through an angle θ_b will exist.

(c) The core of two-dimensional flow will be bounded by the surface bounding the region of influence of vertices A and B (see Fig. 1), the points of intersection of the leading edge and the two side edges of the upper surface of the cowl. The flow spills over the side edges and ultimately, for large enough values of x^1, disturbances due to spillage affect the flow over the full span of the upper surface. The numerical studies described later, in Section 6.5, were undertaken to determine if the numerical methods described in this paper would predict these disturbances.

6.3. *The Numerical Model of the Intake Cowl Shape*

The numerical method based on finite difference approximations to the equations of motion cannot produce accurate results in the immediate neighborhood of the sharp leading edge and the sharp side-edges bounding the upper surface of the cowl. In fact, no fully numerical method will be accurate in these regions, and the non-linearity of the equations of motion prohibits an analytic treatment of flow near to the side edges at least.

To exercise control over the magnitude of numerical truncation errors in the neighborhood of sharp edges, a model of the given shape was produced by rounding the edges. Figure 2 shows the effect of rounding the side edges by means of a circular arc of constant radius δ in planes $x^1 =$ constant. Figure 3 shows the effect of rounding at the leading edge of the upper surface of the given cowl:

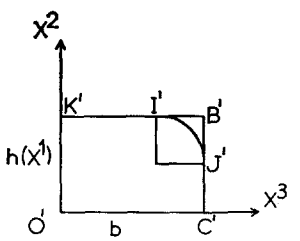

FIG. 2. Modifications to the cross sectional shapes in planes $x^1 =$ constant. $O'K'B'C' =$ original rectangular section. $O'K'I'J'C' =$ modified section.

$K''M''$ represents trace of upper surface of the given cowl;

$L''M''$ represents trace of streamline from uniform flow intersecting the leading edge of the given cowl at K'';

$N''Q''$ represents the modified upper surface of the cowl.

The curve $N''Q''$ is a second order polynomial in x^1 chosen so that $R''N'' = h_0$,

$S''Q'' = h_0 + (x^1)_2 \tan\theta_b$, $dx^2/dx^1 = 0$ at N'' and $dx^2/dx^1 = \tan\theta_b$ at Q''. The values of $(x^1)_1$ and $(x^1)_2$ must satisfy the relation $(x^1)_2 = -(x^1)_1$. The effect of rounding the leading edge is, of course, to extend the intake shape forward by an amount $(x^1)_2$.

In practice the magnitude of the modelling parameters $(x^1)_1$, $(x^1)_2$ and δ will be quite small. Experience has shown that choosing them to be too small leads to

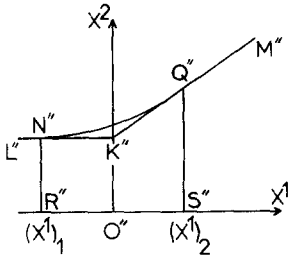

FIG. 3. Modification to cross sectional shapes in planes $x^3 =$ constant ($|x^3| \leqslant b$).

breakdown of the calculation procedure. The value should be chosen just large enough to avoid such breakdowns. Section 6.5 contains satisfactory numerical values for a case that we have studied.

6.4. *Working Region for Calculations*

In order to use the numerical method described in this paper, functions having the form $x^i = x^i(\eta^1, \eta^2, \eta^3)$, $i = 1, 2, 3$ have to be defined in such a way that the region of x-space in which the flow is to be calculated is mapped into a simple region of η-space in which calculations are carried out. This region is called the working space. The functions defining the mapping have to be chosen so that boundary surfaces of the region in x-space are mapped into planes in η-space.

For the intake cowl shape of Section 6.1, with the modifications described in Section 6.3 the transformation defined by the following functions has the required characteristics:

$$\left.\begin{aligned} x^1 &= \eta^1, \\ x^2 &= \eta^3(h(\eta^1) - \delta)/(\eta^3)_1, \\ x^3 &= b + \eta^2, \end{aligned}\right\} \qquad 0 \leqslant \eta^3 \leqslant (\eta^3)_1,$$

$$\left.\begin{aligned} x^1 &= \eta^1, \\ x^2 &= h(\eta^1) - \delta + (\eta^2 + \delta)\sin\left[\frac{((\eta^3) - (\eta^3)_1)\pi/2}{(\eta^3)_2 - (\eta^3)_1}\right], \\ x^3 &= b - \delta + (\eta^2 + \delta)\cos\left[\frac{((\eta^3) - (\eta^3)_1)\pi/2}{(\eta^3)_2 - (\eta^3)_1}\right], \end{aligned}\right\} \qquad (\eta^3)_1 \leqslant \eta^3 \leqslant (\eta^3)_2, \quad (1)$$

$$\left.\begin{aligned} x^1 &= \eta^1, \\ x^2 &= \eta^2 + h(\eta^1), \\ x^3 &= \left[\frac{(\eta^3) - (\eta^3)_3}{(\eta^3)_2 - (\eta^3)_3}\right](b - \delta), \end{aligned}\right\} \qquad (\eta^3)_2 \leqslant \eta^3 \leqslant (\eta^3)_3,$$

where

$$h = \begin{cases} h_0 , & \eta^1 < (\eta^1)_1 , \\ h_0 + \dfrac{0.5 \tan \theta_b (\eta^1 - (\eta^1)_1)^2}{(\eta^1)_2 - (\eta^1)_1} , & (\eta^1)_1 \leqslant \eta^1 \leqslant (\eta^1)_2 , \\ h_0 + \eta^1 \tan \theta_b , & \eta^1 \geqslant (\eta^1)_2 . \end{cases} \tag{2}$$

The quantities $(\eta^1)_1$, $(\eta^1)_2$, $(\eta^3)_1$, $(\eta^3)_2$ and $(\eta^3)_3$ are constants such that $(\eta^1)_1 = (x^1)_1$ and $(\eta^1)_2 = (x^1)_2$. The quantities $(\eta^3)_1$ and $(\eta^3)_2$, together with δ, $(x^1)_1$ and $(x^1)_2$ may have values chosen by the user of the method. For fixed finite difference mesh lengths, $\Delta\eta^1$ and $\Delta\eta^2$, the choice of $(x^1)_1$ will determine the number of finite difference points over the rounded leading edge region. The choice of values $(\eta^3)_1$, $(\eta^3)_2$ and $(\eta^3)_3$ will determine the total number of mesh points ($(\eta^3)_3/\Delta\eta^3$ must be an integer) in the η^3-direction and the number of points in the η^3-direction over the upper surface, over the rounding of the upper surface, and over the side-wall of the intake cowl.

The transformation defined by Eqs. (1) and (2) have the effect illustrated in Fig. 4. The part of the surface $\eta^2 = 0$ such that $\eta^1 \geqslant (\eta^1)_1$ and $0 \leqslant \eta^3 \leqslant (\eta^3)_3$ is the image in the working region of the part of the modified cowl surface that lies in the region $x^3 \geqslant 0$.

The procedure outlined in Section 5 can be used to solve the finite difference equations in the wedge-shaped working region defined by the inequalities (see Fig. 5)

$$\begin{aligned} \eta^1 &\geqslant (\eta^1)_1 , \\ 0 \leqslant \eta^2 &\leqslant k(\eta^1 - (\eta^1)_1), \\ 0 \leqslant \eta^3 &\leqslant (\eta^3)_3 . \end{aligned} \tag{3}$$

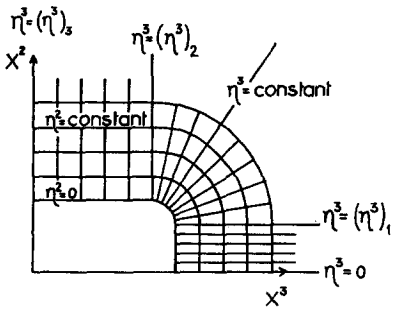

FIG. 4. Traces of the surfaces η^2 = constant and η^3 = constant in a plane x^1 = constant.

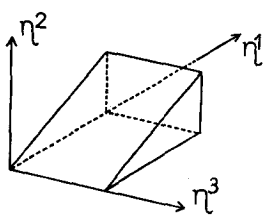

FIG. 5. Wedge-shaped working region in η-space defined by inequalities (3).

The mesh size $\Delta\eta^2$ is chosen so that $\Delta\eta^2 = k\,\Delta\eta^1$, and k itself is chosen so that the computations are stable and so that the dependent variables at points on $\eta^2 = k(\eta^1 - (\eta^1)_1)$ have the same values as those in the uniform stream. On $\eta^2 = 0$, the boundary condition of zero flow through the surface of the intake cowl is applied. On the surfaces $\eta^3 = 0$ and $\eta^3 = (\eta^3)_3$, which correspond to the planes $x^2 = 0$ and $x^3 = 0$ respectively, appropriate symmetry conditions are applied.

6.5. *Numerical Results*

Figure 6 shows comparisons between calculated values, linear theory values and measured values of pressure along the top centre line, *KM* (see Fig. 1), of the intake cowl. The calculated values have been obtained for a shape, of the general form described in Section 6.1, with

$$\begin{aligned} b &= 0.08854167, \\ h_0 &= 0.02083025, \\ \theta_b &= 3.8°, \end{aligned} \tag{4}$$

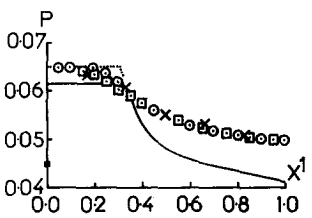

FIG. 6. Comparison of calculated values, linear theory values and measured values of pressure along the top centre line of the intake. ■, free stream pressure; ⊡, Calculated value, $(\eta^3)_3 = 0.0157$; ⊙, Calculated value, $(\eta^3)_3 = 0.02198$; ×, measured value; ——, linear theory; ···, exact theoretical solution.

and for which

$$\delta = 0.01, \qquad \text{and} \qquad (x^1)_2 = 0.0125 \tag{5}$$

in a flow of $M_\infty = 4.0$.

One set of results was obtained with

$$\begin{aligned} \Delta\eta^1 &= 0.005, \\ \Delta\eta^2 &= 0.005, \\ \Delta\eta^3 &= 0.000785, \\ (\eta^3)_1 &= 0.005235988, \\ (\eta^3)_2 &= 0.01047198, \\ (\eta^3)_3 &= 0.0157, \end{aligned} \tag{6}$$

so that in each plane $\eta^1 =$ constant there were 8 mesh points on the intake side-wall, 7 on the rounded part of the model surface, and 8 on the flat upper part of the cowl surface.

A second set of numerical results was obtained by adjusting the value of $(\eta^3)_3$ from 0.0157 to 0.02198 so that with $\Delta\eta^3 = 0.000785$ there were 8 mesh points on the intake side-wall, 7 on the rounded part, and 16 on the upper part of the cowl surface.

In the numerical calculations, h_0 is small compared with b because the experimental results [17] available for comparison with calculated results were obtained using an intake wedge rather than a realistic intake cowl shape. Nevertheless, our view is that the successful results obtained for this problem are indicative of the quality of results that would be obtained for any intake for the general class described in Section 6.1. In the calculations that produced the numerical results given here, we effectively assumed constant entropy by using the equation $(\partial/\partial\eta^1)(p/\rho^\gamma) = 0$.

The linear theory results in Fig. 6 were produced by treating the upper surface of the intake cowl as a plane wing with zero thickness. This is regarded as a reasonable assumption in the case considered here.

Figures 7, 8 and 9 show the variation of pressure on the cowl upper surface with x^3 for three values of x^1. Numerical results are shown for the two different mesh point distributions described earlier. The difference between the linear theory and the exact value for pressure on the surface of a wedge of semi-angle 3.8° indicates that non-linear effects are significant. The good agreement between the exact value for pressure

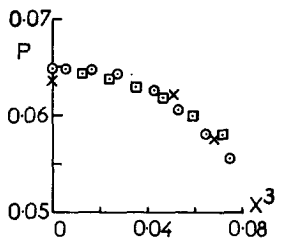

FIG. 7. Pressure distributions on the cowl upper surface, $x^1 = 0.167$. ⊡, calculated value, $(\eta^3)_3 = 0.0157$; ⊙, calculated value, $(\eta^3)_3 = 0.02198$; ×, experimental value.

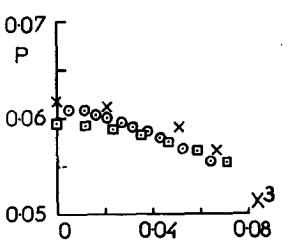

FIG. 8. Pressure distributions on the cowl upper surface, $x^1 = 0.333$. ⊡, calculated value, $(\eta^3)_3 = 0.0517$; ⊙, calculated value, $(\eta^3)_3 = 0.02198$; ×, experimental value.

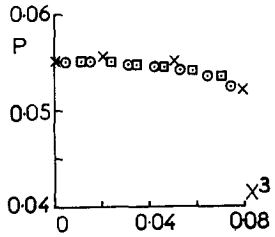

FIG. 9. Pressure distributions on the cowl upper surface, $x^1 = 0.5$. ⊡, calculated value, $(\eta^3)_3 = 0.0157$; ⊙, calculated value, $(\eta^3)_3 = 0.02198$; ×, experimental value.

immediately downstream of the leading edge fairing was interpreted as an indication that the finite difference mesh size $\Delta\eta^2 = 0.005$ was satisfactory. In the absence of experimental results for comparison the good agreement between the numerical results with 21 and 29 mesh points in the η^3-direction, in the latter case there are more points on the cowl surface, would have been interpreted as an indication that the finer of the two finite difference mesh point distributions was satisfactory.

The close agreement between the theoretical results and the experimental results provides additional evidence of both satisfactory accuracy of the computed results, and satisfactory performance of the numerical procedure as a whole.

In the neighborhood of the surface delineating the region of influence of the side edge of the cowl surface, the exact solution of the inviscid flow equations has a discontinuous slope. This discontinuity leads to large truncation errors in the numerical solution in which the discontinuity is smoothed. The expected form of the exact theoretical solution has been filled in on a dotted line in Fig. 6. The computing time for a typical calculation of 200 steps with 21 mesh points in the η^3-direction was 342 seconds on the IBM 360/195 computer.

7. OTHER NUMERICAL RESULTS

Figures 10 and 11 are graphs showing some additional results obtained using the computational algorithms of this paper. This figure shows that the algorithm produces results in agreement with those obtained by Chu [2], who used a characteristics

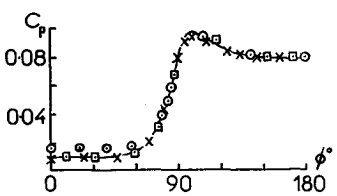

FIG. 10. Pressure distribution on the surface of an elliptic cone (axis ratio 2:1, incidence 4°, $M_\infty = 5.8$). ——, present method (shock treated as a discontinuity); ×, Chu [2]; ⊡, South and Klunker [18]; ⊙, Chapkis [19].

method, and by South and Klunker [18], who used the method of lines, for an elliptic cone. For this problem the bow shock wave was treated as a discontinuity.

The shock capturing capability of the method is illustrated by graphs in Fig. 11. For an elliptic cone cylinder configuration, an embedded shock wave was detected at a station $\eta^1 = 0.168$, as described by Walkden and Evans [20] and then this shock wave was fitted as a discontinuity in the region $\eta^1 > 0.168$. The same flow

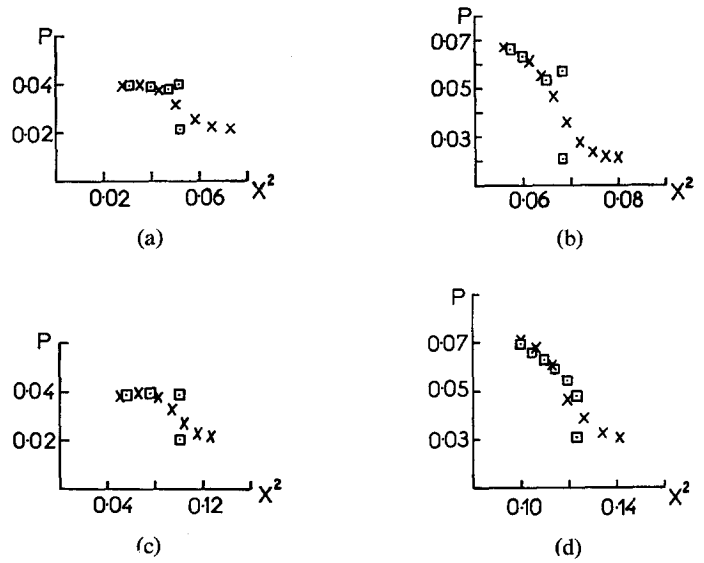

FIG. 11. Pressure variation with distance from the surface of an elliptic cone-cylinder, $M_\infty = 5.8$. ×, shock capturing; ⊡, shock fitted as a discontinuity. (a) $\eta^1 = 0.168$, $\varnothing = 0°$. (b) $\eta^1 = 0.168$, $\varnothing = 90°$. (c) $\eta^1 = 0.38$, $\varnothing = 0°$. (d) $\eta^1 = 0.38$, $\varnothing = 90°$.

field was also calculated by using the method as a shock-capturing algorithm. Figures 11c and 11d show that the shock capturing and shock fitting results compare well at $\eta^1 = 0.38$ after more than 106 integration steps. The elliptic cone cylinder configuration used has major and minor axes described by equations of the form

$$C(x^1) = \begin{cases} 0.1 \tan\theta, & x^1 < -0.1, \\ (0.1 + 2.5(x^1 + 0.1)^2) \tan\theta, & -0.1 \leqslant x^1 \leqslant 0.1, \\ (0.1 + x^1) \tan\theta, & x^1 > 0.1 \end{cases} \tag{1}$$

where $\theta = 11.80°$ or $5.96°$ for the major and minor axes respectively.

8. Closing Remarks

The study of the intake cowl problem described in Section 6 was first undertaken three years ago in order to determine if the general method of this paper provided

a satisfactory procedure for calculating steady supersonic flow fields. The results obtained, some of which are presented in this paper, were encouraging and subsequently the method has been used to calculate flow fields produced by a variety of shapes under different conditions. Fuselage/cockpit canopy combinations, the tip of a rotating/translating helicopter blade, wings, and general cone problems are examples of problems to which the method of this paper has been applied successfully. Satisfactory results for certain of these problems have been presented already [21], but these investigations will be reported fully at a later date. The good agreement between theory and experiment for the intake cowl problem considered in detail here, and the variety of other problems for which satisfactory results have been obtained, leads us to conclude that the method of this paper is satisfactory and is versatile, in the sense that it can quickly be adapted to deal with a wide variety of different supersonic flow problems.

At present, the main obstacle to investigating supersonic flow fields produced by the most complicated of real aircraft shapes is the problem of describing, to the computer, in an appropriate format, geometric details of the boundaries of such shapes and details of co-ordinate surfaces in the space surrounding such shapes. The specification of formats for the data and computer programs to produce large volumes of data in the required format is one area where more work is needed in order to further investigate and improve general computing procedures such as that described here.

APPENDIX 1

Expressions for h_1, h_2, h_3 and r_1, r_2, r_3, k_4 (see Section 2) for Cartesian, cylindrical polar and spherical polar co-ordinate systems are given in the table below.

	Co-ordinate system		
	Cartesian	Cylindrical polar	Spherical polar
h_1	1	1	1
h_2	1	1	x^1
h_3	1	x^2	$x^1 \sin(x^2)$
r_1	0	0	$\{(u_2)^2 + (u_3)^2\}/x^1$
r_2	0	$(u_3)^2/x^2$	$\{(u_3)^2 \cot(x^2) - u_1u_2\}/x^1$
r_3	0	$-u_2u_3/x^2$	$-\{u_2u_3 \cot(x^2) + u_1u_3\}/x^1$
k_4	0	$-u_2/x^2$	$-\{2u_1 + u_2 \cot(x^2)\}/x^1$

APPENDIX 2

Elements of the matrices A, B and C (see Section 3).

$$A = \begin{pmatrix} v^1 & 0 & 0 & 1/\rho \\ 0 & v^1 & 0 & 0 \\ 0 & 0 & v^1 & 0 \\ g^{11} & g^{12} & g^{13} & v^1/\gamma p \end{pmatrix}, \tag{A2.1}$$

$$B = \begin{pmatrix} v^2 & 0 & 0 & 0 \\ 0 & v^2 & 0 & 1/\rho \\ 0 & 0 & v^2 & 0 \\ g^{12} & g^{22} & g^{23} & v^2/\gamma p \end{pmatrix}, \tag{A2.2}$$

$$C = \begin{pmatrix} v^3 & 0 & 0 & 0 \\ 0 & v^3 & 0 & 0 \\ 0 & 0 & v^3 & 1/\rho \\ g^{13} & g^{23} & g^{33} & v^3/\gamma p \end{pmatrix}. \tag{A2.3}$$

ACKNOWLEDGMENTS

The authors gratefully acknowledge assistance received from E.L. Goldsmith of *RAE* Bedford who supplied the experimental results cited, from the Ministry of Defence who provided financial support for telecommunication links, and from the *SRC* who provided computing facilities on their *IBM* 360/195 computer.

REFERENCES

1. T. D. TAYLOR, *AGARDograph* n187 (1974).
2. C. W. CHU, Northrop Corporation Aircraft Division, NOR 72-182, 1973.
3. D. S. BUTLER, *Proc. Roy. Soc. London Ser. A* **255** (1960), 232.
4. P. D. LAX, *Comm. Pure Appl. Math.* **7** (1954), 159.
5. P. KUTLER AND H. LOMAX, *J. Spacecr. Rockets* **8** (1974), 1175.
6. F. MARCONI AND M. SALAS, *Comput. Fluids* **1** (1973), 185.
7. G. MORETTI, B. GROSSMAN, AND F. MARCONI, *AIAA Paper* **72-192** (1972).
8. R. W. MACCORMACK, *AIAA Paper* **69-354** (1969), 1.
9. F. WALKDEN AND P. CAINE, *Int. J. Numer. Methods Eng.* **5** (1972), 151.
10. N. N. YANENKO, "The Method of Fractional Steps," Springer-Verlag, New York, 1971.
11. F. WALKDEN AND P. CAINE, On the application of a pseudo-viscous method to the computation of supersonic flow in an axisymmetric or two-dimensional duct, "Symposium on Internal Flows," University of Salford, C19-27, 1971.
12. F. WALKDEN, G. T. LAWS, AND P. CAINE, *AIAA J.* **5** (1974), 642.
13. P. R. GARABEDIAN AND D. G. KORN, Aeronautical Research Council, Teddington, Middlesex, ARC 33 047 (1971).
14. J. R. STRATTON, "Electromagnetic Theory," pp. 38–47, McGraw-Hill, London, 1941.
15. R. COURANT, E. ISAACSON, AND M. REES, *Comm. Pure Appl. Math.* **5** (1952), 243–255.
16. P. CAINE, MSc. Dissertation, University of Salford, 1977.

17. E. L. GOLDSMITH, private communication, 1974.
18. J. C. SOUTH AND E. B. KLUNKER, *NASA Sp. Publ.* **288** (1970), 131.
19. R. L. CHAPKIS, *J. Aerosp. Sci.* **28** (1961), 844.
20. F. WALKDEN AND D. EVANS, On the detection of Shock waves in steady two- or three-dimensional supersonic gas flows, "Fifth International Conference on Numerical Methods in Fluid Dynamics, Twente University of Technology, Netherlands, 1976."
21. F. WALKDEN, Supersonic flows, *in* "Proceeding of a Conference on Computational Methods and Problems in Aeronautical Fluid Dynamics, Academic Press, London 1976," pp. 354–382.